

1 A climatic control on reorganization of ocean circulation
2 during the mid-Cenomanian Event and Cenomanian–
3 Turonian oceanic anoxic event (OAE-2): Nd-isotope
4 evidence

5 **Xin-Yuan Zheng^{1*}, Hugh C. Jenkyns¹, Andrew S. Gale², David J. Ward³, and**
6 **Gideon M. Henderson¹**

7 *¹Department of Earth Sciences, University of Oxford, South Parks Road, Oxford OX1*
8 *3AN, UK*

9 *²School of Earth and Environmental Sciences, University of Portsmouth, Burnaby*
10 *Road, Portsmouth PO1 3QL, UK*

11 *³Department of Earth Sciences, The Natural History Museum, Cromwell Road,*
12 *London SW7 5BD, UK*

13

14 The published version of this manuscript is available at:
15 [http://geology.geoscienceworld.org/content/44/2/151.full?](http://geology.geoscienceworld.org/content/44/2/151.full?ijkey=npQ4l4zQq1lno&keytype=ref&siteid=gsgeology)
16 [ijkey=npQ4l4zQq1lno&keytype=ref&siteid=gsgeology](http://geology.geoscienceworld.org/content/44/2/151.full?ijkey=npQ4l4zQq1lno&keytype=ref&siteid=gsgeology)

17

18

19

20

21

22

23 *E-mail: xzheng75@wisc.edu.

ABSTRACT

Although ocean circulation plays a vital role in the climate system, its response to major carbon-cycle perturbations during the mid-Cretaceous, including Mid-Cenomanian Event I (MCE I) and Cenomanian–Turonian oceanic anoxic event (OAE 2), is poorly constrained. Here we present Nd-isotope evidence for episodic increases in the influence of boreal seawater in the European epicontinental sea during MCE I. The start of this circulation reorganization lagged the onset of the $\delta^{13}\text{C}$ positive excursion defining MCE I. This sequence of change is similar to that observed during OAE 2 in the same area, showing a consistent response of regional circulation to changes in the global carbon cycle. Brief intervals of invasion of boreal fauna to mid-latitude seas, two during MCE I and one during OAE 2 (Plenus Cold Event), always started after the influence of boreal seawater was enhanced, implying a slower biological response to climate cooling, rather than passive transport of fauna by boreal waters. The lack of an Nd-isotope positive excursion in our record across MCE I supports a volcanic origin for prominent increases in seawater Nd-isotope values found in the European epicontinental sea and tropical Atlantic during OAE 2. The observed tight circulation–carbon cycle coupling may help the upper ocean replenish nutrients from deep waters and/or volcanic sources, providing a critical feedback allowing continuation of MCE I and OAE 2 over long durations.

INTRODUCTION

The mid-Cenomanian event I (MCE I, ~96 Ma) and Cenomanian–Turonian oceanic anoxic event (OAE 2, ~94 Ma) signify two major carbon-cycle perturbations that lasted for ~200 and ~500 ky, respectively (Paul et al., 1994; Sageman et al., 2006). Both events are characterized by a widely recorded marine $\delta^{13}\text{C}$ positive excursion, implying periods of unusually high productivity and excessive organic-carbon burial in the ocean (Paul et al., 1994; Jenkyns, 2010). Contrary to a $>2\text{‰}$ $\delta^{13}\text{C}$ excursion and prevalent ocean anoxia during OAE 2 (Jenkyns, 2010), MCE I was accompanied by a smaller ($\sim 1\text{‰}$) $\delta^{13}\text{C}$ excursion and only local deoxygenation (Paul et al., 1994; Coccioni and Galeotti, 2003). This event, however, shows many features in common with OAE 2, including migration of boreal fauna to mid-latitude seas and transient climate cooling (Paul et al., 1994; Gale and Christensen, 1996; Voigt et al., 2004; van Helmond et al., 2014). MCE I has, consequently, been considered as a precursor to OAE 2 (Coccioni and Galeotti, 2003; Friedrich et al., 2009).

High productivity conditions assumed to characterize both events required increased nutrient supply to the upper ocean. In the case of OAE 2, an accelerated hydrological cycle, intensified silicate weathering and intense large igneous province (LIP) volcanism may have served as direct or indirect nutrient sources (Blättler et al., 2011; Pogge von Strandmann et al., 2013; Du Vivier et al., 2014; van Helmond et al., 2014). Upwelling of nutrient-rich deep waters may also have played a role during both events (Voigt et al., 2004; Jenkyns, 2010). The mechanism that sustained nutrient supply to the upper ocean over the long periods of these events remains unknown. Ocean circulation must have been involved as a driver, as it directly distributes nutrients in seawater, but its exact role is unclear.

This study uses Nd isotopes (expressed by ϵ_{Nd}) to track changes of ocean circulation in the European epicontinental sea during MCE I. Watermasses in the ocean are tagged by characteristic ϵ_{Nd} from surrounding continents, and their ϵ_{Nd} signatures are maintained during circulation (e.g. Jeandel et al., 2007). Distinct seawater ϵ_{Nd} values in major ocean basins during the mid-Cretaceous allow for tracing of watermasses with different origins (Pacific: ~ -2 – -4 ; Tethys: ~ -4 – -8 ; Atlantic: ~ -6 – -8 ; European epicontinental sea: ~ -10) (e.g. Puc  at et al., 2005; MacLeod et al., 2008; Robinson et al., 2010).

Nd isotopes revealed a change in ocean circulation in the European epicontinental sea in response to transient climate cooling during OAE 2 (Zheng et al., 2013). Here we examine whether such a circulation–climate coupling is unique to OAE 2 by tracing seawater ϵ_{Nd} in the same area during the analogous MCE I. In addition, prominent ϵ_{Nd} increases were observed in the European epicontinental sea and tropical Atlantic (Demerara Rise) during OAE 2, and were explained by either a change of circulation or advection of radiogenic Nd from intense volcanism during the event (MacLeod et al., 2008; Martin et al., 2012, Zheng et al., 2013). These possibilities may be resolved by tracing seawater ϵ_{Nd} across MCE I, for which there is no accompanying evidence of major volcanic pulses.

SECTION BACKGROUND

We sampled an ~ 11 m-thick section exposed at Lydden Spout in Folkestone (UK, 51.10°N , 1.26°E). The section comprises a sequence of foraminiferal–nannofossil chalk–marl couplets, which have been numbered and considered to represent ~ 20 kyr-precession cycles (Paul et al., 1994; Gale, 1995). A double-peak $\delta^{13}\text{C}$ positive excursion defining MCE I was reported from an outcrop at Abbot’s

Cliff (Paul et al., 1994), ~200 m away to the west of the outcrop studied here. The section was deposited in shallow waters (<1000 m) in a pelagic epicontinental environment at the junction of the Boreal Sea, Tethys and proto-North Atlantic during the mid-Cretaceous (Fig. 1).

Two widely traceable beds in the section, the lower one at the basal couplet B41 (*arlesiensis* Bed) and the upper one at the basal couplet C1 (*primus* Bed), contain abundant faunas of boreal affinity (Fig. 2) (Paul et al., 1994; Gale 1995), notably two species of bivalve, *Chlamys arlesiensis* (Woods) and *Oxytoma seminudum* (Dames), and a nektonic belemnite, *Actinocamax primus* (Arkhangelsky). These boreal species also occur widely in European basins at levels equivalent to Bed 4–8 of the Plenus Marls during OAE 2 (Fig. 2), where *A. primus* is replaced by the descendant species *A. plenus* (Blainville) (Gale and Christensen, 1996).

MATERIALS AND METHODS

Bulk-chalk $\delta^{13}\text{C}$ was measured every ~5 cm. Nd isotopes were measured on fish debris collected from 23 stratigraphic levels at ~50-cm spacing, and supplemented by measurements on carbonate fractions of bulk chalk, extracted by acetic acid, from 10 additional levels. Paired fish debris and carbonates from 8 stratigraphic levels were measured to compare ϵ_{Nd} values of the two archives. To assess the possible use of carbonates in chalk sections for seawater ϵ_{Nd} reconstruction, ϵ_{Nd} was also measured on carbonates from 10 stratigraphic levels in a European reference chalk section for OAE 2 at Eastbourne, and then compared with the published fish-debris ϵ_{Nd} values from identical levels (Zheng et al., 2013). Details on extraction of fish debris and carbonates, and analytical protocols are available in the GSA Data Repository.

RESULTS

Carbon isotopes rise from $\sim 1.9\text{‰}$ near the base of couplet B38 towards peak values of $\sim 2.5\text{‰}$ in the *arlesiensis* Bed at couplet B41 (Fig. 2). After a trough of $\sim 2.2\text{‰}$ at couplet B42–B43, $\delta^{13}\text{C}$ rises to $\sim 2.5\text{‰}$ again towards the top of the *primus* Bed at couplet C1 before decreasing from the upper couplet C2. The stratigraphic position of the double-peak $\delta^{13}\text{C}$ positive excursion agrees with that reported from the nearby Abbot's Cliff (Paul et al., 1994), although $\delta^{13}\text{C}$ values differ between the two sections probably due to subtle differences in lithology or local diagenesis.

Fish debris and carbonates from the same stratigraphic levels recorded identical ϵ_{Nd} values (Fig. 2), validating construction of a composite ϵ_{Nd} record using data from both archives. Nd isotopes start to decrease from background values of ~ -9 at the uppermost couplet B39, one couplet above the onset of the $\delta^{13}\text{C}$ rise at lower couplet B38. It continues to decrease towards a minima of ~ -10 in the *arlesiensis* Bed during the first $\delta^{13}\text{C}$ rise. Above that, ϵ_{Nd} returns to background values while $\delta^{13}\text{C}$ decreases from its first peak. Up-section, ϵ_{Nd} decreases again from the upper couplet B42, and reaches minima of ~ -10 within the *primus* Bed, being followed by an abrupt ϵ_{Nd} reversal to background values, and then by a ~ 0.7 -unit decrease roughly at the level of the second $\delta^{13}\text{C}$ peak. It finally recovers to background values at the end of the $\delta^{13}\text{C}$ excursion.

The stratigraphy of the ϵ_{Nd} negative excursions corresponds closely with the boreal-fauna levels, but the onset of the first and second ϵ_{Nd} drop predates the first appearance of these fossils at the *arlesiensis* Bed and the *primus* Bed respectively, although the second ϵ_{Nd} excursion is interrupted by a rapid ϵ_{Nd} reversal within the

primus Bed, resulting in a double-peak ϵ_{Nd} negative excursion over this faunal interval.

DISCUSSION

Origin of the ϵ_{Nd} record across MCE I

Fish debris incorporates seawater Nd on the seafloor (Martin and Scher, 2004), thereby recording bottom-water ϵ_{Nd} values. High Nd concentration of fish debris (mostly >200 ppm, Table DR2) and low clay content (<20 wt%, Paul et al., 1994) in the studied section should minimize overprint of fish-debris ϵ_{Nd} due to possible diagenetic release of detrital Nd: an assertion supported by the lack of co-variation between ϵ_{Nd} and lithology (Fig. 2).

Acid leachates of sediments may yield ϵ_{Nd} distinct from seawater values, depending on sediment compositions and depositional settings (Charbonnier et al., 2012), but carbonates of chalk in this study must record seawater ϵ_{Nd} , because they have values identical to those in fish debris from the same stratigraphic levels (Fig. 2). The good agreement between the two archives may result from low detrital contents of chalk, highlighting the possible use of carbonates as a simple substitute for future seawater ϵ_{Nd} reconstruction in Cretaceous chalk sections.

Nd-isotope inferred reorganizations of ocean circulation during MCE I

Both tropical and Norwegian seaways were open during the mid-Cretaceous (Fig. 1), so seawater ϵ_{Nd} in the European epicontinental sea may have been affected by upper ocean circulation connecting the Tethys and North Atlantic, and by boreal seawater. Except for low ϵ_{Nd} values (~-11 to -16) found on Demerara Rise due to local influence of Guyana Shield input (Martin et al., 2012), relatively high ϵ_{Nd} values

(~-4 to -9) found in shallow and intermediate waters at mid-latitudinal North Atlantic sites and east Tethys during the Cretaceous have been explained by advection of Pacific seawater with high ϵ_{Nd} values via a putative circumglobal current that dominated the upper ocean circulation at mid-latitudes (Fig. 1) (Puc  at et al., 2005; Martin et al., 2012). Circulation flowing between the Atlantic and Tethys may, therefore, have had a radiogenic ϵ_{Nd} signature. By contrast, boreal seawater likely had low ϵ_{Nd} values, because of weathering input from surrounding Precambrian continents characterized by ϵ_{Nd} between ~-17 and -30 (Jeandel et al., 2007). A seawater ϵ_{Nd} value of ~-17 has been found from the boreal realm during the Cretaceous (Puc  at et al., 2005).

Recurrent ϵ_{Nd} negative excursions during MCE I (Fig. 2) are interpreted to reflect transient increases in the influence of boreal seawater in the European epicontinental sea. Enhanced weathering of surrounding Precambrian continents may lower seawater ϵ_{Nd} values, but the recurrent, rapid and reversible nature of the ϵ_{Nd} negative excursions is difficult to reconcile with changes in continental weathering. Furthermore, pulses of intensified weathering are not supported by temperature reconstructions that show little climate warming during MCE I (e.g. Voigt et al., 2004; Ando et al., 2009).

Modelling results suggest that ocean circulation in the European epicontinental sea was sensitive to tectonics or sea-level changes during the mid-Cretaceous (Poulsen et al., 1998). However, the transient and recurrent circulation reorganizations are neither compatible with slow and irreversible tectonic movements, nor a sea-level control, because all inferred circulation changes occurred during assumed sea-level rise (Fig. 2).

A climatic control on circulation reorganizations during MCE I and OAE 2

The onset of the period with episodic increases of boreal influence in bottom waters in the European epicontinental sea, marked by the first ϵ_{Nd} negative excursion, lagged the onset of $\delta^{13}\text{C}$ rise of MCE I. This lead–lag relationship is identical to that observed for OAE 2 in the same area (Fig. 2), where enhanced influence of boreal seawater, suggested by a similar 1-unit ϵ_{Nd} negative excursion, occurred after the onset of the $\delta^{13}\text{C}$ rise of OAE 2 (Zheng et al., 2013). These records show a consistent response of regional circulation to carbon-cycle changes during both events.

Enhanced organic carbon burial and silicate weathering during OAE 2 sequestered atmospheric CO_2 , leading to intermittent climate cooling (Forster et al., 2007; Blättler et al., 2011; Jarvis et al., 2011; Pogge von Strandmann et al., 2013; van Helmond et al., 2014). The onset of circulation change during OAE 2 coincided with such a cooling (Fig. 2) (Zheng et al., 2013), reflecting a prompt circulation response to climate-induced fluctuations in the latitudinal thermal gradient and/or the wind system (Forster et al., 2007; Zheng et al., 2013).

The same climate forcing may explain circulation reorganizations during MCE I, because enhanced organic carbon burial during this event can in principle cause episodic atmospheric CO_2 drawdown, albeit at a smaller magnitude compared to OAE 2. Transient $\sim 2^\circ\text{C}$ cooling during MCE I is suggested by $\delta^{18}\text{O}$ records from the European epicontinental sea and North Atlantic (Voigt et al., 2004), although conclusive evidence showing a global cooling during the event remains lacking. The broad correlation between ϵ_{Nd} drops and $\delta^{13}\text{C}$ peaks during MCE I, similarly observed during OAE 2, is compatible with a link between circulation changes and marine carbon burial (Fig. 2).

Implications for the cause of the ϵ_{Nd} positive excursion during OAE 2

An obvious difference in ϵ_{Nd} records from the European epicontinental sea for MCE I and OAE 2 is the presence of an ϵ_{Nd} positive excursion during OAE 2 (Fig. 2). An unusually large (~8-unit) ϵ_{Nd} positive excursion was also found on Demerara Rise in the tropical Atlantic during OAE 2 (MacLeod et al., 2008; Martin et al., 2012). The ϵ_{Nd} increases during OAE 2 have been considered to reflect either climate-induced intensification of high ϵ_{Nd} waters from the Tethys or North Atlantic (Martin et al., 2012), or advection of radiogenic Nd released from LIP volcanisms under anoxic conditions (Zheng et al., 2013). Considering analogous carbon-cycle variations and the similar response of European epicontinental circulation during both events, if an ϵ_{Nd} positive excursion during OAE 2 resulted purely from a circulation change, it would be predicted for MCE I. However, no ϵ_{Nd} increase is seen across the MCE I either in the European epicontinental sea or on Demerara Rise (Jiménez Berrocoso et al., 2010), supporting a volcanic origin for the ϵ_{Nd} positive excursion during OAE 2 (Zheng et al., 2013).

A climatic control on boreal faunal migration during MCE I and OAE 2

The three boreal faunal events, two during MCE I and one during OAE 2 (i.e. Plenus Cold Event; Paul et al., 1994; Gale and Christensen, 1996), can be explained either by passive transport of fauna due to enhanced export of boreal waters to the mid-latitudes, or by a biological response to climate-induced cooling of the ocean. The ϵ_{Nd} records of MCE I and OAE 2 imply enhanced influence of boreal seawater in the European epicontinental sea, but the first appearance of boreal faunas for the three faunal intervals invariably took place after the influence of boreal seawater was increased (Fig. 2), favoring the latter explanation for these faunal events. Ocean

circulation responded more quickly to climate forcing, because boreal faunas may not migrate southwards until climate-induced cooling of global ocean could offset the likely warming of boreal waters at the mid-latitudes due to entrainment of low-latitude seawater. Variable boreal-water influence during faunal migration, implied by the double-peak ϵ_{Nd} excursion in the *primus* Bed (Fig. 2), also supports a more sensitive response of ocean circulation to climate fluctuations.

Implications for the maintenance of MCE I and OAE 2

This study shows a prompt response of ocean circulation in the European epicontinental sea to carbon-cycle changes during MCE I and OAE 2. Such a high circulation–climate sensitivity is not revealed by previous modelling results (Poulsen et al., 2001), and may explain transient circulation changes suggested previously for other parts of the ocean during both events (Ando et al., 2009; Jiménez Berrocoso et al., 2010; Jarvis et al., 2011). The tight carbon cycle–circulation coupling, if operating on a large scale, could help replenish surface waters with nutrients from deep waters and/or LIP sources, providing a critical positive feedback that sustained high productivity of MCE I and OAE 2 over protracted periods.

ACKNOWLEDGMENTS

Supported by the Oxford University Clarendon Scholarship to X.-Y. Zheng. We thank Stuart Robinson, Martin Frank, Emmanuelle Pucéat, Jochen Erbacher and an anonymous reviewer for helpful comments.

REFERENCES CITED

- Ando, A., Huber, B.T., MacLeod, K.G., Ohta, T., and Khim, B.-K., 2009, Blake Nose stable isotopic evidence against the mid-Cenomanian glaciation hypothesis: *Geology*, v. 37, p. 451–454, doi:10.1130/G25580A.1.
- Blättler, C.L., Jenkyns, H.C., Reynard, L.M. and Henderson, G.M., 2011, Significant increases in global weathering during Oceanic Anoxic Events 1a and 2 indicated by calcium isotopes, *Earth and Planetary Science Letters*, v. 309, p. 77–88, doi:10.1016/j.epsl.2011.06.029.
- Charbonnier, G., Pucéat, E., Bayon, G., Desmares, D., Dera, G., Durlet, C., Deconinck, J.-F., Amédéo, F., Gourlan, A., Pellenard, P., and Bomou, B., 2012, Reconstruction of the Nd isotope composition of seawater on epicontinental seas: testing the potential of Fe–Mn oxyhydroxide coatings on foraminifera tests for deep-time investigations: *Geochimica et Cosmochimica Acta*, v. 99, p. 39–56, doi:10.1016/j.gca.2012.09.012.
- Coccioni, R., and Galeotti, S., 2003, The mid-Cenomanian Event: prelude to OAE 2: *Palaeogeography, Palaeoclimatology, Palaeoecology*, v. 190, p. 427–440, doi:10.1016/S0031-0182(02)00617-X.
- Du Vivier, A.D.C., Selby, D., Sageman, B.B., Jarvis, I., Gröcke, D.R., and Voigt, S., 2014, Marine $^{187}\text{Os}/^{188}\text{Os}$ isotope stratigraphy reveals the interaction of volcanism and ocean circulation during Oceanic Anoxic Event 2: *Earth and Planetary Science Letters*, v. 389, p. 23–33, doi:10.1016/j.epsl.2013.12.024.
- Forster, A., Schouten, S., Moriya, K., Wilson, P.A., and Sinninghe Damsté, J.S., 2007, Tropical warming and intermittent cooling during the Cenomanian/Turonian oceanic anoxic event 2: sea surface temperature records from the equatorial Atlantic: *Paleoceanography*, v. 22, PA1219, doi:10.1029/2006PA001349.
- Friedrich, O., Erbacher, J., Wilson, P.A., Moriya, K., and Mutterlose, J., 2009, Paleoenvironmental changes across the Mid Cenomanian Event in the tropical Atlantic Ocean (Demerara Rise, ODP Leg 207) inferred from benthic foraminiferal assemblages: *Marine Micropaleontology*, v. 71, p. 28–40, doi:10.1016/j.marmicro.2009.01.002.
- Gale, A.S., 1995, Cyclostratigraphy and correlation of the Cenomanian stage of Europe: *Special Publications of the Geological Society*, v. 85, p. 177–197, doi: 10.1144/GSL.SP.1995.085.01.11.
- Gale, A.S., and Christensen, W., 1996, Occurrence of the belemnite *Actinocamax plenus* in the Cenomanian of SE France and its significance: *Bulletin of the Geological Society of Denmark*, v. 43, p. 68–77.
- Jarvis, I., Lignum, J.S., Gröcke, D.R., Jenkyns, H.C. and Pearce, M.A., 2011, Black shale deposition, atmospheric CO₂ drawdown, and cooling during the Cenomanian–Turonian Oceanic Anoxic Event: *Paleoceanography*, v. 26, PA3201, doi:10.1029/2010PA002081.
- Jeandel, C., Arsouze, T., Lacan, F., Téchiné, P., and Dutay, J.-C., 2007, Isotopic Nd compositions and concentrations of the lithogenic inputs into the ocean: a compilation, with an emphasis on the margins: *Chemical Geology*, v. 239, p. 156–164, doi:10.1016/j.chemgeo.2006.11.013.
- Jenkyns, H.C., 2010, Geochemistry of oceanic anoxic events: *Geochemistry Geophysics Geosystems*, v. 11, Q03004, doi:10.1029/2009GC002788.
- Jiménez Berrocoso, Á., MacLeod, K., Martin, E., Bourbon, E., Londoño, C., and Basak, C., 2010, Nutrient trap for Late Cretaceous organic-rich black shales in the tropical North Atlantic: *Geology*, v. 38, no. 12, p. 1111–1114, doi:10.1130/G31195.1.

MacLeod, K.G., Martin, E.E., and Blair, S.W., 2008, Nd isotopic excursion across Cretaceous ocean anoxic event 2 (Cenomanian-Turonian) in the tropical North Atlantic: *Geology*, v. 36, p. 811–814, doi:10.1130/G24999A.1.

Martin, E.E., MacLeod, K.G., Jiménez Berrocoso, A., and Bourbon, E., 2012, Water mass circulation on Demerara Rise during the Late Cretaceous based on Nd isotopes: *Earth and Planetary Science Letters*, v. 327–328, p. 111–120, doi:10.1016/j.epsl.2012.01.037.

Martin, E.E., and Scher, H.D., 2004, Preservation of seawater Sr and Nd isotopes in fossil fish teeth: bad news and good news: *Earth and Planetary Science Letters*, v. 220, p. 25–39, doi:10.1016/S0012-821X(04)00030-5.

Paul, C.R.C., Mitchell, S.F., Marshall, J.D., Leafy, P.N., Gale, A.S., Duane, A.M., and Ditchfield, P.W., 1994, Palaeoceanographic events in the Middle Cenomanian of Northwest Europe: *Cretaceous Research*, v. 15, p. 707–738, doi:10.1006/cres.1994.1039.

Pogge von Strandmann, P.A.E., Jenkyns, H.C., and Woodfine, R.G., 2013, Lithium isotope evidence for enhanced weathering during Oceanic Anoxic Event 2: *Nature Geoscience*, v. 6, p. 668–672, doi:10.1038/ngeo1875.

Poulsen, C.J., Barron, E.J., Arthur, M.A., and Peterson, W.H., 2001, Response of the Mid-Cretaceous global oceanic circulation to tectonic and CO₂ forcings: *Paleoceanography*, v. 16, p. 576–592, doi:10.1029/2000PA000579.

Poulsen, C.J., Seidov, D., Barron, E.J., and Peterson, W.H., 1998, The impact of paleogeographic evolution on the surface oceanic circulation and the marine environment within the mid-Cretaceous Tethys: *Paleoceanography*, v. 13, p. 546–559, doi:10.1029/98PA01789.

Pucéat, E., Lécuyer, C., and Reisberg, L., 2005, Neodymium isotope evolution of NW Tethyan upper ocean waters throughout the Cretaceous: *Earth and Planetary Science Letters*, v. 236, p. 705–720, doi:10.1016/j.epsl.2005.03.015.

Robinson, S.A., Murphy, D.P., Vance, D., and Thomas, D.J., 2010, Formation of “Southern Component Water” in the Late Cretaceous: evidence from Nd-isotopes: *Geology*, v. 38, p. 871–874, doi:10.1130/G31165.1.

Sageman, B.B., Meyers, S.R., and Arthur, M.A., 2006, Orbital time scale and new C-isotope record for Cenomanian-Turonian boundary stratotype: *Geology*, v. 34, p. 125–128, doi: 10.1130/G22074.1.

van Helmond, N.A.G.M., Sluijs, A., Reichert, G.-J., Sinninghe Damsté, J.S., Slomp, C.P., and Brinkhuis, H., 2014, A perturbed hydrological cycle during Oceanic Anoxic Event 2: *Geology*, v. 42, p. 123–126, doi:10.1130/G34929.1.

Voigt, S., Gale, A.S., and Flögel, S., 2004, Midlatitude shelf seas in the Cenomanian-Turonian greenhouse world: temperature evolution and North Atlantic circulation: *Paleoceanography*, v. 19, PA4020, doi:10.1029/2004PA001015.

Wilmsen, M., 2003, Sequence stratigraphy and palaeoceanography of the Cenomanian Stage in northern Germany: *Cretaceous Research*, v. 24, p. 525–568, doi:10.1016/S0195-6671(03)00069-7.

Zheng, X.-Y., Jenkyns, H.C., Gale, A.S., Ward, D.J., and Henderson, G.M., 2013, Changing ocean circulation and hydrothermal inputs during Ocean Anoxic Event 2 (Cenomanian–Turonian): evidence from Nd-isotopes in the European shelf sea: *Earth and Planetary Science Letters*, v. 375, p. 338–348, doi:10.1016/j.epsl.2013.05.053.

Figure 1. Paleogeographic map of the mid-Cretaceous (Jarvis et al. 2011), showing Lydden Spout and Eastbourne (star), sites mentioned in the text (circle) with seawater ϵ_{Nd} , and the general circulation pattern (arrow) (Puc  at et al., 2005; Martin et al., 2012). Ce–Cenomanian; Co–Coniacian; Maa–Maastrichtian.

Figure 2. Results of $\delta^{13}C$ and ϵ_{Nd} from the Lydden Spout section across MCE I. (A) red circles–carbonate $\delta^{13}C$; thick red line–10-point moving average; red dashed line–pre-MCE $\delta^{13}C$ values; grey line–carbonate $\delta^{13}C$ from Abbot’s Cliff (Paul et al., 1994); red arrow–the initial $\delta^{13}C$ rise; grey band–MCE I. (B) thick orange line– ϵ_{Nd} curve (fish debris: orange circle; carbonates: open black circle; mean values: half-filled orange circle; paired fish debris and carbonates: pink square and blue diamond); orange arrow–the onset of the first ϵ_{Nd} drop. (C) black curve–sea-level reconstruction (Wilmsen, 2003). Graded yellow bands–boreal-fauna levels with darker yellow indicating the two beds where boreal faunas are abundant (Paul et al., 1994). (D) Results of $\delta^{13}C$ (grey) and ϵ_{Nd} (orange) from the Eastbourne section across OAE 2 (grey band) are shown for comparison (Zheng et al., 2013). Red bar–a volcanic pulse coincident with the positive ϵ_{Nd} excursion; yellow band–levels of boreal faunas (the Plenus Marl Beds 4–8; i.e. Plenus Cold Event); blue bar–transient cooling based on combined geochemical and faunal evidence from the same section (Zheng et al., 2013). Green bar in (B) and (D)–pre-event ϵ_{Nd} background; dashed lines “a” and “b” in (A) (B) and (D)–the onset of the $\delta^{13}C$ rise and the onset of circulation reorganization, respectively.

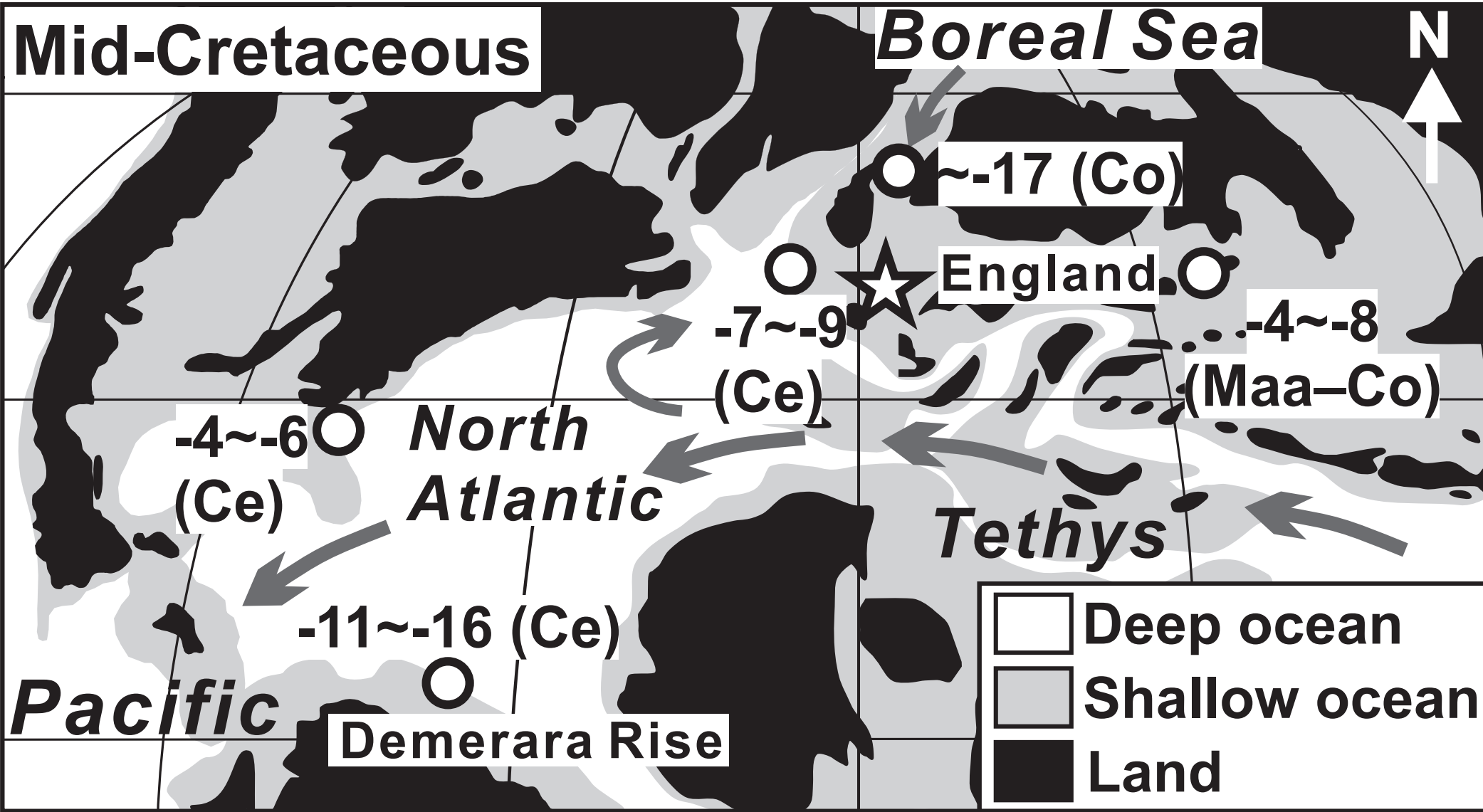
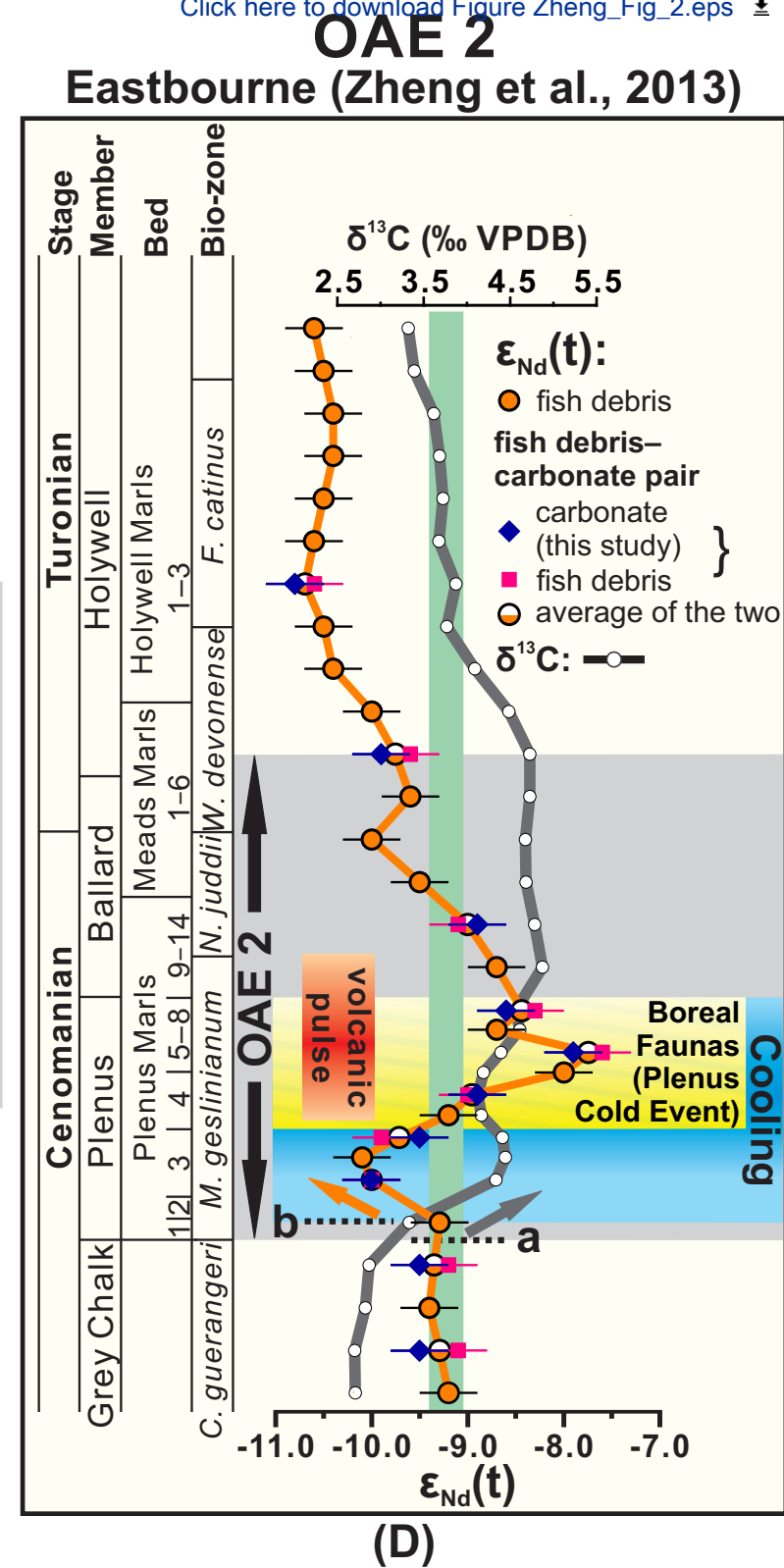
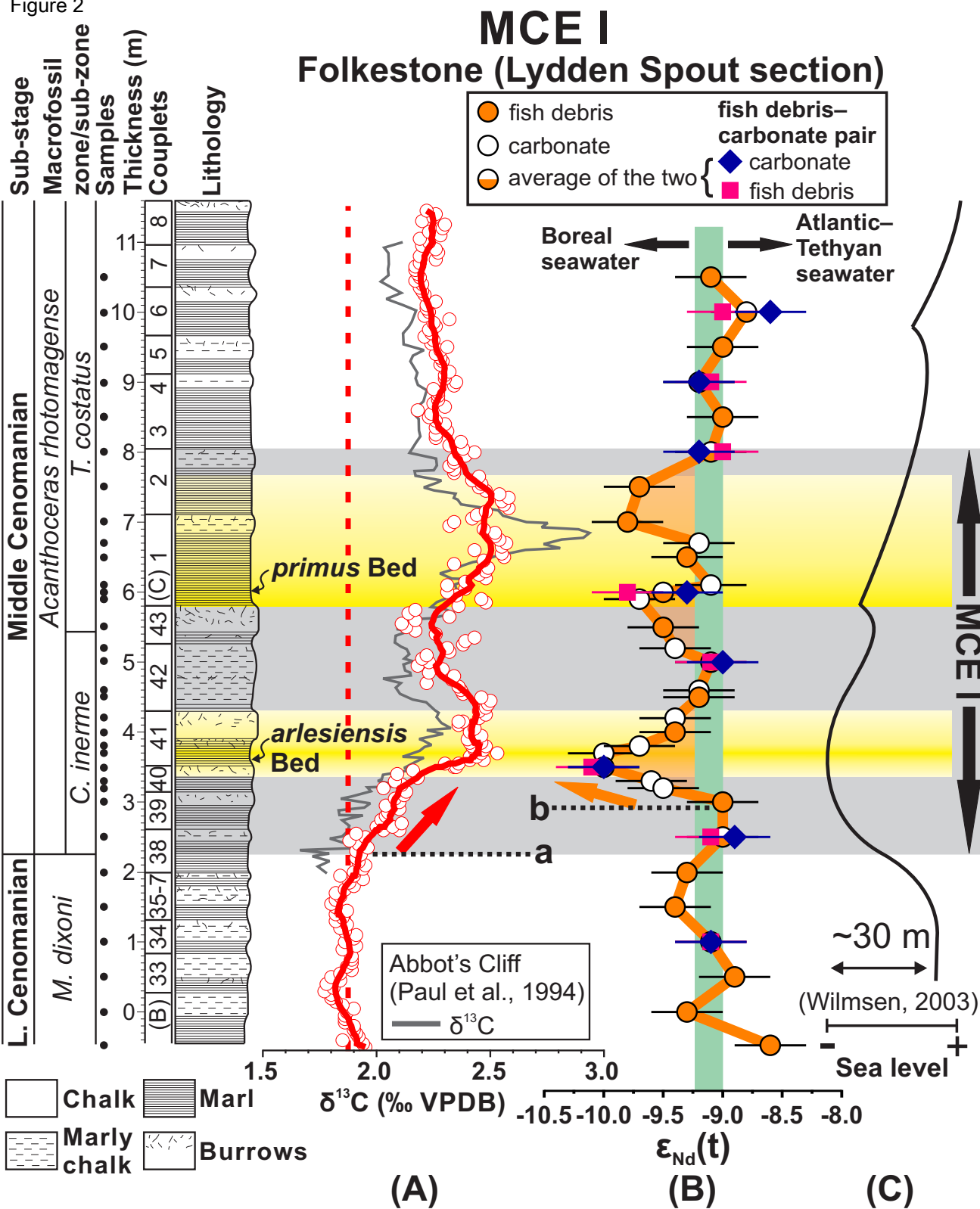


Figure 2



Supplementary materials

A climatic control on reorganization of ocean circulation during the mid-Cenomanian Event (MCE I) and Cenomanian–Turonian oceanic anoxic event (OAE 2): Nd-isotope evidence

Xin-Yuan Zheng, Hugh C. Jenkyns, Andrew S. Gale,
David J. Ward, and Gideon M. Henderson

1. Sample preparation

Fish debris was extracted from bulk chalks using a method described in Zheng et al. (2013). Carbonate fractions of bulk chalk were removed by dissolving in ~7.5% (v/v) formic acid, buffered to a pH of ~3.2 with ~7.5% (v/v) calcium acetate solution, for 1–3 days. Fish debris was then handpicked from the residues under a binocular microscope. Fish debris was cleaned by a reductive–oxidative protocol to remove Fe–Mn oxides and attached fine clays (Boyle, 1981; Boyle and Keigwin, 1985; Rosenthal et al., 1997), and then dissolved in 6 M quartz-distilled HCl at ~120°C for at least 12 h. Dissolved fish-debris samples were split into two aliquots for measurement of Nd isotopes and Sm/Nd ratios.

Carbonate fractions of bulk chalk from several stratigraphic levels were also measured for Nd isotopes to increase temporal resolution of the ϵ_{Nd} record across MCE I. Large chunks of chalk (> 10 g) were ground into powder using an agate pestle and mortar. About 5 g of powder was leached using 10% (v/v) distilled acetic acid at

room temperature for ~2 h before being centrifuged, and supernatant liquid was then taken for elemental and Nd isotopic analysis.

2. Analytical protocols

2.1. Bulk chalk $\delta^{13}\text{C}$

Bulk chalk $\delta^{13}\text{C}$ was measured using a VG Isogas Prism II mass spectrometer with an on-line VG Isocarb common acid bath preparation system. Carbonate powders were dosed with acetone and dried at 60°C for at least 30 minutes. In the instrument they were reacted with purified phosphoric acid at 90°C. Calibration to the VPDB standard via NBS-19 was made daily using the in-house (NOCZ) Carrara Marble standard. Reproducibility of $\delta^{13}\text{C}$ measurement is better than 0.1‰ (1 σ).

2.2. Nd isotopes, Nd/Sm ratios and in-growth correction

Nd isotopes were measured on an MC-ICP-MS (Nu plasma) after purification of Nd with a two-stage ion-exchange chromatographic separation. The first stage used AG 50W-X12 resin (Bio-Rad, 200–400 mesh, H form) and HCl as an eluent to separate REEs from major matrix ions, and the second stage adopted AG 50W-X4 (Bio-Rad, 200–400 mesh, ammonium form) and α -hydroxyisobutyric acid (α -HIBA) as an eluent to separate Nd from other REEs. The procedural blank of <50 pg Nd was negligible compared to >120 ng Nd processed through column separation. Instrumental mass bias was corrected by using $^{146}\text{Nd}/^{144}\text{Nd} = 0.7219$ and the exponential fractionation law. Repeated measurement of JNdi-1 yielded $^{143}\text{Nd}/^{144}\text{Nd} = 0.512099 \pm 0.000017$ (n=301, 2 σ), which is in good agreement with the published consensus value (Tanaka et al., 2000). Repeated analysis of a fish bone composite standard yielded $^{143}\text{Nd}/^{144}\text{Nd} = 0.512364 \pm 0.000013$ (n=21, 2 σ), which also agrees

with inter-laboratory calibration results (Scher and Delaney, 2010). Long-term reproducibility of Nd-isotope analysis is estimated to be $\sim 0.3 \epsilon_{\text{Nd}}$ unit (2σ).

All ϵ_{Nd} values reported in this study were corrected for radiogenic in-growth of ^{143}Nd from ^{147}Sm . Sm/Nd ratios that were measured on an HR-ICP-MS (Element 2) using indium as an internal standard. Repeated measurement on a gravimetrically prepared REE solution indicated that the measured Sm/Nd ratios agreed with its gravimetric value within $\sim 1\%$. Long-term reproducibility of the Sm/Nd ratio, based on measurements of the gravimetrically prepared REE solution and a fish bone composite standard, is estimated to be better than 1% (1σ).

For ^{143}Nd in-growth correction, the age model was based on cyclostratigraphy that considers each chalk–marl couplet to be controlled by a 20 kyr-precession cycle (Gale et al., 1999), and the base of the *C. inermis* Zone was tied to 96.50 Ma according to the Geological Time Scale (GTS) 2012 (Gradstein et al., 2012).

References

- Boyle E. A. (1981) Cadmium, zinc, copper, and barium in foraminifera tests. *Earth Planet. Sci. Lett.* **53**, 11-35.
- Boyle E. A. and Keigwin L. D. (1985) Comparison of Atlantic and Pacific paleochemical records for the last 215,000 years: changes in deep ocean circulation and chemical inventories. *Earth Planet. Sci. Lett.* **76**, 135-150.
- Gale A. S., Young J. R., Shackleton N. J., Crowhurst S. J. and Wray D. S. (1999) Orbital tuning of Cenomanian marly chalk successions: towards a Milankovitch time-scale for the Late Cretaceous. *Philosophical Transactions of the Royal Society of London. Series A: Mathematical, Physical and Engineering Sciences* **357**, 1815-1829.
- Gradstein F. M., Ogg J. G., Schmitz M. and Ogg G. (2012) The Geologic Time Scale 2012. 2-Volume Set (1st edition). Elsevier.
- Rosenthal Y., Boyle E. A. and Labeyrie L. (1997) Last Glacial Maximum Paleochemistry and Deepwater Circulation in the Southern Ocean: Evidence From Foraminiferal Cadmium. *Paleoceanography* **12**, 787-796.
- Scher H. D. and Delaney M. L. (2010) Breaking the glass ceiling for high resolution Nd isotope records in early Cenozoic paleoceanography. *Chem. Geol.* **269**, 329-338.
- Tanaka T., Togashi S., Kamioka H., Amakawa H., Kagami H., Hamamoto T., Yuhara M., Orihashi Y., Yoneda S., Shimizu H., Kunimaru T., Takahashi K., Yanagi

84 T., Nakano T., Fujimaki H., Shinjo R., Asahara Y., Tanimizu M. and
85 Dragusanu C. (2000) JNdi-1: a neodymium isotopic reference in
86 consistency with LaJolla neodymium. *Chem. Geol.* **168**, 279-281.
87 Zheng X.-Y., Jenkyns H. C., Gale A. S., Ward D. J. and Henderson G. M. (2013)
88 Changing ocean circulation and hydrothermal inputs during Ocean Anoxic
89 Event 2 (Cenomanian–Turonian): evidence from Nd-isotopes in the
90 European shelf sea. *Earth Planet. Sci. Lett.* **375**, 338-348.

Table DR1

Results of bulk-carbonate $\delta^{13}\text{C}$

Height (m)	$\delta^{13}\text{C}$ (‰ _{V-PDB})	Height (m)	$\delta^{13}\text{C}$ (‰ _{V-PDB})	Height (m)	$\delta^{13}\text{C}$ (‰ _{V-PDB})
-0.50	1.95	2.35	1.96	4.80	2.34
-0.45	1.94	2.40	1.92	4.85	2.23
-0.40	1.85	2.45	1.88	4.90	2.29
-0.35	1.92	2.50	1.95	4.95	2.18
-0.30	1.91	2.55	1.91	5.00	2.23
-0.25	1.90	2.60	2.10	5.05	2.20
-0.20	1.90	2.60	2.03	5.10	2.22
-0.15	1.86	2.65	2.00	5.15	2.32
-0.10	1.86	2.65	2.07	5.20	2.31
-0.05	1.86	2.70	2.11	5.25	2.38
0.00	1.87	2.75	2.02	5.30	2.39
0.05	1.90	2.80	2.04	5.35	2.43
0.10	1.85	2.85	2.05	5.40	2.26
0.15	1.82	2.90	2.10	5.45	2.17
0.20	1.80	2.95	2.04	5.50	2.13
0.25	1.80	3.00	2.10	5.55	2.11
0.30	1.77	3.05	2.08	5.60	2.17
0.35	1.81	3.10	2.12	5.65	2.32
0.40	1.78	3.15	2.13	5.70	2.14
0.45	1.84	3.20	2.03	5.75	2.17
0.50	1.80	3.25	2.11	5.80	2.36
0.55	1.84	3.30	2.08	5.85	2.48
0.60	1.89	3.35	2.18	5.90	2.46
0.65	1.87	3.40	2.09	5.95	2.35
0.70	1.89	3.45	2.16	6.00	2.31
0.75	1.89	3.50	2.34	6.05	2.39
0.80	1.89	3.50	2.35	6.10	2.31
0.85	1.87	3.55	2.36	6.15	2.39
0.90	1.85	3.55	2.30	6.20	2.48
0.95	1.91	3.60	2.47	6.25	2.45
1.00	1.86	3.60	2.41	6.30	2.48
1.05	1.90	3.65	2.41	6.35	2.49
1.10	1.91	3.65	2.44	6.40	2.34
1.15	1.86	3.70	2.46	6.45	2.47
1.20	1.84	3.70	2.53	6.50	2.56
1.25	1.87	3.75	2.47	6.55	2.55
1.30	1.82	3.75	2.43	6.60	2.43
1.35	1.85	3.80	2.42	6.65	2.55
1.40	1.82	3.80	2.48	6.70	2.57
1.40	1.82	3.85	2.41	6.75	2.54
1.45	1.84	3.85	2.46	6.80	2.52
1.45	1.87	3.90	2.40	6.85	2.52
1.50	1.82	3.95	2.46	6.90	2.47
1.55	1.80	4.00	2.41	6.95	2.32
1.60	1.82	4.05	2.43	7.00	2.34
1.65	1.84	4.10	2.36	7.05	2.42
1.70	1.82	4.15	2.38	7.10	2.44
1.75	1.86	4.15	2.36	7.15	2.48
1.80	1.90	4.20	2.45	7.20	2.58
1.85	1.88	4.25	2.48	7.25	2.56
1.90	1.94	4.30	2.45	7.30	2.55
1.95	1.84	4.35	2.48	7.35	2.58
1.95	1.90	4.40	2.49	7.40	2.54
2.00	1.90	4.45	2.50	7.45	2.48
2.05	1.94	4.50	2.46	7.50	2.45
2.10	1.95	4.55	2.38	7.55	2.46
2.15	1.92	4.60	2.37	7.60	2.42
2.20	1.91	4.65	2.36	7.65	2.45
2.25	1.93	4.70	2.22	7.70	2.34
2.30	1.91	4.75	2.33	7.75	2.34

Table DR1 (continued)Results of bulk-carbonate $\delta^{13}\text{C}$

Height (m)	$\delta^{13}\text{C}$ (‰ _{V-PDB})	Height (m)	$\delta^{13}\text{C}$ (‰ _{V-PDB})	Height (m)	$\delta^{13}\text{C}$ (‰ _{V-PDB})
7.80	2.32	9.05	2.30	10.35	2.19
7.85	2.34	9.10	2.30	10.40	2.20
7.90	2.34	9.15	2.32	10.45	2.17
7.95	2.39	9.20	2.29	10.50	2.19
8.00	2.43	9.25	2.28	10.55	2.18
8.05	2.38	9.30	2.29	10.60	2.17
8.10	2.32	9.35	2.28	10.65	2.17
8.15	2.37	9.40	2.26	10.70	2.19
8.20	2.26	9.45	2.28	10.75	2.26
8.25	2.26	9.50	2.31	10.80	2.19
8.30	2.31	9.55	2.24	10.85	2.27
8.35	2.26	9.60	2.25	10.90	2.26
8.40	2.30	9.65	2.21	10.95	2.20
8.45	2.26	9.70	2.24	11.00	2.23
8.50	2.23	9.75	2.23	11.05	2.19
8.55	2.24	9.80	2.26	11.10	2.28
8.60	2.18	9.85	2.25	11.15	2.23
8.65	2.30	9.90	2.32	11.20	2.29
8.70	2.25	9.95	2.21	11.25	2.30
8.75	2.27	10.00	2.23	11.30	2.20
8.80	2.27	10.05	2.22	11.35	2.25
8.85	2.27	10.10	2.22	11.40	2.26
8.90	2.25	10.15	2.26	11.45	2.22
8.95	2.34	10.25	2.21		
9.00	2.35	10.30	2.20		

Table DR2

Results of ϵ_{Nd} for MCE I

Sample	Height (m)	Age ^a (Ma)	$^{143}\text{Nd}/^{144}\text{Nd}$ (0)	2σ	$^{147}\text{Sm}/^{144}\text{Nd}$	$\epsilon_{\text{Nd}}(0)$	$\epsilon_{\text{Nd}}(t)^b$	[Nd] (ppm)
FISH DEBRIS								
LS05a	-0.5	96.592	0.512148	0.000005	0.1218	-9.6	-8.6	701
LS04a	0.0	96.575	0.512118	0.000010	0.1268	-10.1	-9.3	1724
LS03a	0.5	96.559	0.512136	0.000009	0.1229	-9.8	-8.9	766
LS02a	1.0	96.542	0.512126	0.000006	0.1221	-10.0	-9.1	6875
LS01a	1.5	96.525	0.512106	0.000009	0.1211	-10.4	-9.4	2930
LS1	2.0	96.508	0.512116	0.000009	0.1208	-10.2	-9.3	857
LS2	2.5	96.492	0.512124	0.000010	0.1224	-10.0	-9.1	203
LS3	3.0	96.475	0.512128	0.000008	0.1205	-9.9	-9.0	572
LS4	3.5	96.458	0.512077	0.000007	0.1266	-10.9	-10.1	3757
LS5	4.0	96.441	0.512107	0.000010	0.1154	-10.4	-9.4	1133
LS6	4.5	96.425	0.512122	0.000008	0.1231	-10.1	-9.2	888
LS7	5.0	96.408	0.512124	0.000010	0.1204	-10.0	-9.1	382
LS8	5.5	96.391	0.512102	0.000009	0.1190	-10.4	-9.5	738
LS9	6.0	96.374	0.512092	0.000008	0.1259	-10.7	-9.8	60
LS10	6.5	96.358	0.512113	0.000011	0.1196	-10.2	-9.3	291
LS1a	7.0	96.341	0.512089	0.000007	0.1215	-10.7	-9.8	641
LS2a	7.5	96.324	0.512097	0.000006	0.1238	-10.6	-9.7	95
LS3a	8.0	96.307	0.512128	0.000008	0.1209	-9.9	-9.0	757
LS4a	8.5	96.291	0.512129	0.000011	0.1205	-9.9	-9.0	251
LS5a	9.0	96.274	0.512123	0.000007	0.1223	-10.1	-9.1	191
LS6a	9.5	96.257	0.512127	0.000008	0.1207	-10.0	-9.0	—
LS7a	10.0	96.240	0.512127	0.000007	0.1196	-10.0	-9.0	98
LS8a	10.5	96.224	0.512127	0.000007	0.1217	-10.0	-9.1	855
BULK CARBONATE								
LS02a_carb	1.0	96.542	0.512119	0.000006	0.1146	-10.1	-9.1	—
LS2_carb	2.5	96.492	0.512125	0.000010	0.1034	-10.0	-8.9	—
LSP6_carb	3.2	96.468	0.512100	0.000008	0.1127	-10.5	-9.5	—
LSP7_carb	3.3	96.465	0.512089	0.000007	0.1091	-10.7	-9.6	—
LS4_carb	3.5	96.458	0.512073	0.000009	0.1104	-11.0	-10.0	—
LSP11_carb	3.7	96.451	0.512072	0.000008	0.1132	-11.0	-10.0	—
LSP12_carb	3.8	96.448	0.512091	0.000008	0.1207	-10.7	-9.7	—
LSP16_carb	4.2	96.435	0.512106	0.000008	0.1144	-10.4	-9.4	—
LSP20_carb	4.6	96.421	0.512112	0.000008	0.1115	-10.3	-9.2	—
LS7_carb	5.0	96.408	0.512121	0.000008	0.1092	-10.1	-9.0	—
LSP25_carb	5.2	96.401	0.512107	0.000008	0.1177	-10.3	-9.4	—
LSP31_carb	5.9	96.378	0.512084	0.000008	0.1084	-10.8	-9.7	—
LS9_carb	6.0	96.374	0.512107	0.000009	0.1126	-10.3	-9.3	—
LSP33_carb	6.1	96.371	0.512119	0.000008	0.1161	-10.1	-9.1	—
LSP39_carb	6.7	96.351	0.512109	0.000008	0.1050	-10.3	-9.2	—
LS3a_carb	8.0	96.307	0.512113	0.000007	0.1151	-10.2	-9.2	—
LS5a_carb	9.0	96.274	0.512108	0.000008	0.1061	-10.3	-9.2	—
LS7a_carb	10.0	96.240	0.512141	0.000008	0.1083	-9.7	-8.6	—

^aAge model was based on Gradstein et al. (2012);^b $\epsilon_{\text{Nd}}(t) = \{ [^{143}\text{Nd}/^{144}\text{Nd}_{\text{sample}}(t) / ^{143}\text{Nd}/^{144}\text{Nd}_{\text{CHUR}}(t)] - 1 \} \times 10^4$; $^{143}\text{Nd}/^{144}\text{Nd}(t) = ^{143}\text{Nd}/^{144}\text{Nd}(0) - ^{147}\text{Sm}/^{144}\text{Nd}(0) \times [\text{EXP}(\lambda_{\text{Sm}} \times T) - 1]$; λ_{Sm} (decay constant of ^{147}Sm) = $6.54 \times 10^{-12} \text{ yr}^{-1}$; T: age; $^{147}\text{Sm}/^{144}\text{Nd}_{\text{CHUR}}(0) = 0.1967$, $^{143}\text{Nd}/^{144}\text{Nd}_{\text{CHUR}}(0) = 0.512638$.

Table DR3Results of ϵ_{Nd} in acetic acid extracted carbonates from Eastbourne for OAE 2

Sample	Height ^a (m)	Age ^b (Ma)	Bulk Carbonate				Fish Debris ^c		
			¹⁴³ Nd/ ¹⁴⁴ Nd	2SE	¹⁴⁷ Sm/ ¹⁴⁴ Nd	$\epsilon_{\text{Nd}}(0)$	$\epsilon_{\text{Nd}}(t)$	$\epsilon_{\text{Nd}}(0)$	$\epsilon_{\text{Nd}}(t)$
HC2	1	94.08	0.512103	0.000009	0.1166	-10.4	-9.5	-10.0	-9.1
HC4	3	94.00	0.512092	0.000007	0.1043	-10.7	-9.5	-10.2	-9.2
HC6	5	93.91	0.512080	0.000006	0.1206	-10.9	-10.0	-10.9	-10.0
HC7	6	93.86	0.512104	0.000006	0.1177	-10.4	-9.5	-10.8	-9.9
HC8	7	93.82	0.512129	0.000007	0.1100	-9.9	-8.9	-9.9	-9.0
HC9	8	93.78	0.512187	0.000007	0.1179	-8.8	-7.9	-8.4	-7.5
HC10	9	93.73	0.512157	0.000007	0.1278	-9.4	-8.6	-9.1	-8.3
HC12	11	93.65	0.512127	0.000007	0.1088	-10.0	-8.9	-10.2	-9.2
HC16	15	93.49	0.512072	0.000007	0.0982	-11.0	-9.9	-10.7	-9.7
HC20	19	93.34	0.512030	0.000007	0.1055	-11.9	-10.8	-11.7	-10.7

^aHeight is consistent with Zheng et al. (2013);^bAge model was based on Voigt et al. (2008);^cData were taken from Zheng et al. (2013).